Structural Engineering and Mechanics, Vol. 31, No. 1 (2009) 93-112
DOI: http://dx.doi.org/10.12989/sem.2009.31.1.093

Evaluation of seismic energy demand and its application on design of buckling-restrained braced frames

Hyunhoon Choi and Jinkoo Kim†

Department of Architectural Engineering, Sungkyunkwan University, Suwon, Korea

(Received April 1, 2008, Accepted November 17, 2008)

Abstract. In this study seismic analyses of steel structures were carried out to examine the effect of ground motion characteristics and structural properties on energy demands using 100 earthquake ground motions recorded in different soil conditions, and the results were compared with those of previous works. Analysis results show that ductility ratios and the site conditions have significant influence on input energy. The ratio of hysteretic to input energy is considerably influenced by the ductility ratio and the strong motion duration. It is also observed that as the predominant periods of the input energy spectra are significantly larger than those of acceleration response spectra used in the strength design, the strength demand on a structure designed based on energy should be checked especially in short period structures. For that reason framed structures with buckling-restrained-braces (BRBs) were designed in such a way that all the input energy was dissipated by the hysteretic energy of the BRBs, and the results were compared with those designed by conventional strength-based design procedure.

Keywords: input energy; hysteretic energy; energy-based seismic design; strength-based design.

1. Introduction

During the past few decades, researchers and engineers in earthquake engineering field have been trying to develop innovative seismic design methodologies, which provide predictable seismic performance of structures as potential alternatives to the conventional strength-based seismic design methods. These efforts resulted in the development of some practical design methods considering inelastic responses such as Capacity Spectrum Method (CSM), Displacement-Based Design (DBD) and Energy-Based Design (EBD). Among these design methods, the design procedures of CSM and DBD are proposed in detail and utilized in the engineering practice whereas there is no coincidence of experts' opinions about the procedure of EBD. This study was motivated by this point of view.

The energy-based design approach started from the work of Housner (1956). After publication of his work, a lot of research on energy method has followed; in this paper only a few works are mentioned in the following. Zahrah and Hall (1984) carried out seismic analyses of structures using 8 earthquake records, and reported that the effect of ductility, damping, and post-yield stiffness on the input and hysteretic energy is not significant. Fajfar and Vidic (1994) computed seismic input and hysteretic energy using 40 earthquake records, and found that the input energy and the ratio of

† Associate Professor, Corresponding author, E-mail: jkim12@skku.ac.kr

the hysteretic to input energy decrease as ductility ratio increases. Decanini and Mollaioli (2001) carried out research on the variation of hysteretic to input energy ratio for various soil conditions, hysteresis models, and ductility ratios. For energy-based design of structures, Akbas *et al.* (2001) proposed a procedure in which the seismic input energy demand is dissipated by the accumulated plastic deformation at beam ends. Leelataviwat *et al.* (2002), Kim *et al.* (2004), Choi and Kim (2006a) and Choi *et al.* (2006b) proposed a seismic design method based on the energy balance concept. The neural network model was adopted by Akbas (2006) to predict the hysteretic energy demand in steel moment resisting frames.

Although a lot of research have been carried out in the field of energy-based seismic design, there has yet been discrepancies on some issues, probably due to the differences in the number and characteristics of earthquake records used in the analysis. Also the validity of the energy-based design compared to the conventional strength-based design procedure still needs to be investigated.

In this study seismic analyses of steel structures were carried out to examine the effect of ground motion characteristics such as site conditions, magnitude and strong motion duration of earthquakes, and of the structural characteristics such as natural period, ductility ratio, etc. The results were compared with the previous research works mentioned above. As large number of earthquake records is required to ensure generality of the analysis results, 100 records developed for the SAC Steel Project (Somerville *et al.* 1997) were used in this study. Then framed structures with buckling-restrained-braces (BRBs) were designed in such a way that all the input energy is dissipated by the hysteretic energy of the BRBs, and the performance of the structures were compared with those of structures designed based on the conventional strength-based procedure.

2. Energy equation

The equation of motion of a SDOF structure is written as

$$m\ddot{x} + c\dot{x} + f_s(x,\dot{x}) = -m\ddot{x}_g \tag{1}$$

where m, c, and $f_s(x,\dot{x})$ are the mass, damping coefficient, and recovery force, respectively, and $\ddot{x}_g$ is the ground acceleration. The integration of the above equation with respect to the relative displacement x leads to the following energy equation (Chopra 1995)

$$\int_0^x m\ddot{x}dx + \int_0^x c\dot{x}dx + \int_0^x f_s(x,\dot{x})dx = -\int_0^x m\ddot{x}_g dx \tag{2}$$

By using the relationship $dx = \dot{x}dt$, the above equation can be rewritten as follows

$$\int_0^t m\ddot{x}\dot{x}dt + \int_0^t c(\dot{x})^2 dt + \int_0^t f_s(x,\dot{x})\dot{x}dt = -\int_0^t m\ddot{x}_g\dot{x}dt \tag{3}$$

where the first and the second terms of Eq. (2) or (3) represent the kinetic energy (E_k) and the damping energy (E_d), respectively, and the third term represents the absorbed energy (E_a) composed of the recoverable elastic strain energy (E_s) and the irrecoverable hysteretic energy (E_h). The right-hand-side of the equation represents the input seismic energy (E_i). Therefore the energy balance equation of motion of a SDOF structure is written as

$$E_k + E_d + E_s + E_h = E_i \tag{4}$$

The energy in the above equation is the relative energy based on the relative displacement between the structure and the base. The absolute energy can be estimated using the absolute displacement associated with the earthquake-induced ground motion and the relative displacement. Uang and Bertero (1988) stated that the absolute energy is more reasonable than the relative energy because the absolute energy can take the rigid-body motion into account. Chopra (1995) insisted that the relative energy is more important because the member force of a structure is computed based on the relative displacement and relative velocity. By comparing the absolute and relative energy time histories of SDOF structure for simple pulse excitation, Bruneau and Wang (1996) showed that a conceptual paradox exists in that the absolute input energy can still fluctuate long after the termination of the input excitation. Also they concluded that the relative energy is more meaningful from the viewpoint of engineering interest.

The difference between the relative and the absolute energy is contributed from the difference in input and kinetic energies. However, the total amount of energy becomes the same at the end of the vibration. Also according to Uang and Bertero (1988) the relative and the absolute input energies are almost the same when the natural period of a structure is within the range of 0.3~5.0 second. In the energy-based seismic design the hysteretic energy contributed from the plastic deformation of structural members computed based on the relative displacement is one of the most important design parameters. Therefore in this study the relative energy is used in the formulation of energy equation.

3. Variation of input and hysteretic energy

3.1 Earthquake ground motions used in the analysis

The 100 earthquake records, originally developed in the SAC steel project (Somerville *et al.* 1997) for five different soil conditions such as stiff soil, soft soil, and near-fault conditions in Los Angeles (high seismicity) and Boston (low seismicity) areas, were used in this study. These design level ground motions have 10% probability of exceedance in 50 years. The stiff and the soft soil conditions correspond to the site classes D and E, respectively, in the IBC-2006 format (ICC 2006). For each soil condition 20 earthquake records (10 sets) were used, and in each set of ground motions two horizontal components were provided. Two different soil profiles and three thicknesses of each profile were taken to develop the time histories for soft soil sites. Among the six soil models (one for each combination of soil profile and depth) the time histories for site class D and 30 m depth to firm ground were selected in this study. According to the SAC report by Somerville *et al.* (1997), although the ground motions for near-fault condition were developed considering various faulting mechanisms in the magnitude range of 6 3/4 to 7 1/2 and the closest distance range of 0 to 10 km, these time histories do not represent a statistical sample of near-fault motions. However they insist that the characteristics of the suggested motions are representative of the variability in recorded time histories for a given magnitude, distance, and site condition in empirical ground motion models. The records NF01~NF20 out of the 40 recorded ground motions for near-fault condition were used in this study. The characteristics of motions and the mathematical model used for the simulation process are described in the SAC Report. Figs. 1 and 2 show the 5% damped elastic response spectra of the earthquake records utilized.

In the evaluation of the damage accumulated in a structure as a result of an earthquake, the

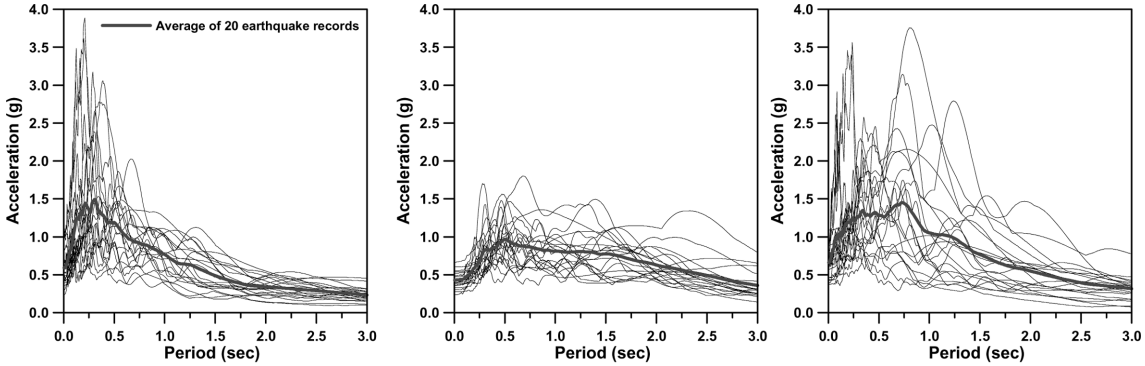

(a) Stiff soil (b) Soft soil (c) Near-fault

Fig. 1 Response spectra of ground motions developed in SAC Project for LA area

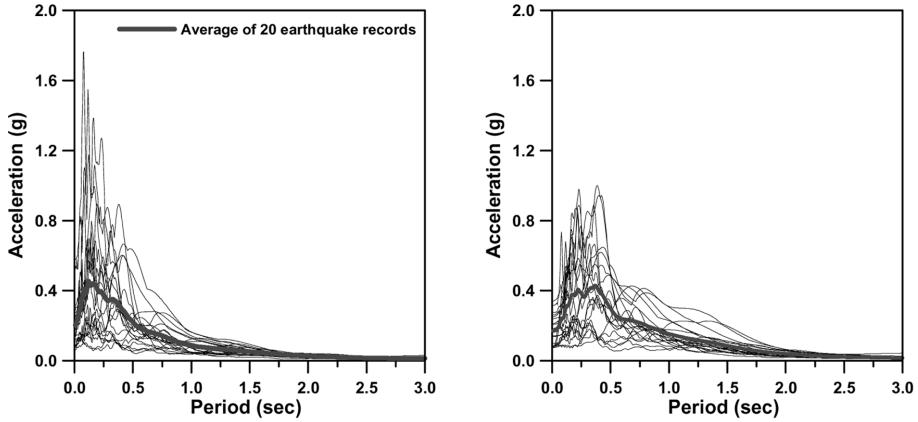

(a) Stiff soil (b) Soft soil

Fig. 2 Response spectra of ground motions developed in SAC Project for Boston area

magnitude of strong motion duration (t_{sd}) of the earthquake is an important factor, which is obtained as follows (Trifunac and Brady 1975)

$$t_{sd} = t_{0.95} - t_{0.05} \tag{5}$$

where $t_{0.05}$ and $t_{0.95}$ denote the time that the Arias intensity (I_A), obtained as follows (Arias 1970), reaches 5% and 95%, respectively

$$I_A = \frac{\pi}{2g}\int_0^{t_{td}} \ddot{x}_g^2(t)dt \tag{6}$$

where t_{td} is the total duration of earthquake, g and $\ddot{x}_g$ are the gravity acceleration and the ground acceleration, respectively. The total and the strong motion durations of the earthquake records used in the analysis are presented in Table 1 and 2, respectively. The earthquake records with long and short strong motion duration were identified; for example, in the earthquakes recorded in stiff soil in Los Angeles; earthquakes with long strong motion duration : LA01, LA02, LA07, LA08, LA09,

Table 1 Total (t_{td}) and strong motion duration (t_{sd}) of earthquake ground motions developed in SAC Steel Project for Los Angeles area

SAC Name	Stiff soil		SAC Name	Soft soil		SAC Name	Near-fault	
	t_{td} (sec)	t_{sd} (sec)		t_{td} (sec)	t_{sd} (sec)		t_{td} (sec)	t_{sd} (sec)
LA01	53.46	24.26	LS01	81.90	25.34	NF01	49.98	18.45
LA02	53.46	24.52	LS02	81.90	23.56	NF02	49.98	17.66
LA03	39.38	8.52	LS03	40.95	12.99	NF03	24.99	9.52
LA04	39.38	**7.09**	LS04	40.95	**8.27**	NF04	24.99	10.68
LA05	39.08	10.80	LS05	40.95	**6.98**	NF05	39.98	**3.26**
LA06	39.08	10.42	LS06	40.95	12.43	NF06	39.98	**5.08**
LA07	79.98	22.26	LS07	81.90	23.44	NF07	59.98	15.82
LA08	79.98	22.24	LS08	81.90	24.14	NF08	59.98	17.10
LA09	79.98	19.66	LS09	81.90	27.22	NF09	20.775	**7.135**
LA10	79.98	20.74	LS10	81.90	26.78	NF10	20.775	10.085
LA11	39.98	11.32	LS11	81.90	12.88	NF11	49.28	13.384
LA12	39.98	**6.40**	LS12	81.90	19.06	NF12	49.28	14.224
LA13	59.98	**5.72**	LS13	81.90	**8.48**	NF13	14.945	**7.015**
LA14	59.98	**5.54**	LS14	81.90	12.50	NF14	14.945	9.545
LA15	14.945	7.80	LS15	20.475	**7.005**	NF15	59.98	**5.84**
LA16	14.945	**7.035**	LS16	20.475	**8.265**	NF16	59.98	**6.08**
LA17	59.98	7.20	LS17	81.90	**5.62**	NF17	59.98	**7.10**
LA18	59.98	**5.30**	LS18	81.90	**6.82**	NF18	59.98	7.94
LA19	59.98	8.56	LS19	81.90	9.62	NF19	40.09	10.66
LA20	59.98	**6.78**	LS20	81.90	12.20	NF20	40.09	13.13

Table 2 Total (t_{td}) and strong motion duration (t_{sd}) of earthquake ground motions developed in SAC Steel Project for Boston area

SAC Name	Stiff soil		SAC Name	Soft soil	
	t_{td} (sec)	t_{sd} (sec)		t_{td} (sec)	t_{sd} (sec)
BO01	29.99	**3.72**	BS01	40.91	**3.80**
BO02	29.99	**4.08**	BS02	40.91	**4.03**
BO03	29.99	**2.56**	BS03	40.91	**2.85**
BO04	29.99	**2.79**	BS04	40.91	**2.75**
BO05	19.255	**4.43**	BS05	40.975	8.24
BO06	19.255	**6.33**	BS06	40.975	8.585
BO07	20.335	8.255	BS07	20.485	7.985
BO08	20.335	8.255	BS08	20.485	7.530
BO09	18.775	9.50	BS09	20.485	11.620
BO10	18.775	9.24	BS10	20.485	11.685
BO11	19.015	11.62	BS11	20.485	8.125
BO12	19.015	11.96	BS12	20.485	**4.860**
BO13	17.755	14.16	BS13	20.485	14.245
BO14	17.755	11.80	BS14	20.485	12.875
BO15	29.57	8.94	BS15	40.97	6.39
BO16	29.57	11.04	BS16	40.97	5.51
BO17	39.05	12.13	BS17	40.97	9.25
BO18	39.05	13.49	BS18	40.97	6.04
BO19	33.29	8.98	BS19	40.97	**4.70**
BO20	33.29	**7.76**	BS20	40.97	**3.66**

Table 3 Average strong motion duration of each set of ground motions

Area	LA			Boston	
Soil type	Stiff soil	Soft soil	Near-fault	Stiff soil	Soft soil
Set of 20 earthquake records (sec)	12.11	14.68	10.49	8.56	7.24
Long strong motion duration (sec)	20.71	24.22	15.68	12.31	10.93
Short strong motion duration (sec)	6.27	7.35	5.93	4.52	3.81

LA10, and LA11; earthquakes with short strong motion duration : LA04, LA12, LA13, LA14, LA16, LA18, and LA20. Table 3 presents the average strong motion duration of each set of ground motions for five different soil conditions.

When sufficient records were not available in the SAC time histories for each soil condition, broadband strong motions were simulated. According to the research by Teran-Gilmore and Jirsa (2004) using long duration narrow-banded ground motions recorded in the lake zone of Mexico City, which have predominant period around 2.0 sec, the maximum plastic energy demands for Mexico soft soil are about two to three times larger than those for the SAC ground motions for LA area. Bojórquez and Ruiz (2004) also utilized the narrow-band motions recorded in the Valley of Mexico to investigate the effect of low-cycle fatigue on the ductility capacity. These results obtained from narrow-band motions recorded in very soft soil were compared with those obtained from SAC records.

3.2 Input energy and hysteretic energy

From analyses using 8 earthquake records, Zahrah and Hall (1984) concluded that ductility demand (μ) does not have a significant influence on the earthquake input energy (E_i). Uang and Bertero (1988) also showed that the input energy spectra are generally insensitive to the level of ductility ratio for El Centro record (1940, N00E) and San Salvador record (1986, N90E). More researchers (Akiyama 1985, Nakashima *et al*. 1996) reported similar observations. Based on the assumption that input energy is independent of system parameters such as viscous damping, ductility and strength level, Cruz and López (2000) suggested simple expressions of the plastic energy, expressed as a fraction of the input energy, calculated in terms of normalized input power, which incorporates five single-degree-of-freedom (SDOF) and two multi-degree-of-freedom (MDOF) structures. However, according to the analysis results using mean response of 40 earthquake records by Fajfar and Vidic (1994), the input energy decreases as ductility increases for period range larger than about 0.4 second. On the other hand, though the input energy was not much affected by the change of ductility for short periods less than 0.4 second, it was observed that the input energy increases as ductility increases. Also Decanini and Mollaioli (2001) showed that ductility has a significant influence on input energy. Using 10 earthquake records each with short and long duration of strong motion, Khashaee *et al*. (2003) concluded that as the ductility increases, the influence of the duration of strong motion on the input energy spectra becomes more significant, particularly in the vicinity of the predominant period.

It can be observed in the review of the previous research that there is inconsistency whether ductility has a negligible effect on input energy or not. Much part of the discrepancy is originated from how the results were obtained; e.g. results from individual record or from averaging many results obtained from individual records. Considering the non-stationary nature of earthquakes, it

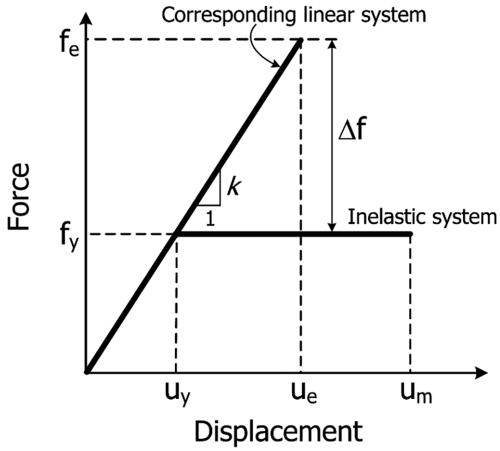

Fig. 3 Force-displacement relationship of an elastoplastic system and its corresponding linear system

seems to be more reasonable to use mean values using ensemble of earthquake records in the investigation of the effect of various parameters on the seismic input and hysteretic energy. In this study the input and hysteretic energy were computed for 100 SDOF systems using the nonlinear analysis program code NONSPEC (Mahin and Lin 1983). The analysis model structures, the natural period of which ranges from 0.05 second to 5.0 second, have bi-linear force-displacement relationship with zero post-yield stiffness. Damping ratio was assumed to be 5% of the critical damping. Time-history analyses were carried out and the energy responses for the 20 earthquakes in each site condition were averaged. For SDOF structures with various natural periods and target ductility ratios energy response spectra can be constructed according to the procedure as follows:

i) Determine target ductility (μ_t) and damping ratio, and select earthquake ground motion
ii) Select a value for period (T_n) of SDOF system
iii) Compute f_e, $f_y(=f_e-\Delta f)$ and u_y of the system as shown in Fig. 3. Where f_e is the peak force in the corresponding linear system, f_y and u_y are the yield force and displacement of elastoplastic system with the same period, respectively.
iv) Obtain maximum displacement (u_m) using nonlinear time-history analysis for selected SDOF system.
v) Compute ductility ratio ($\mu = u_m/u_y$). Repeat steps (iii) and (iv) with increased Δf until μ converges on μ_t. If $\mu = \mu_t$, then calculate energy responses for system with selected f_y and u_y.
vi) Repeat analysis steps (ii) to (v) for the period range of interest.

Figs. 4 and 5 present the variation of earthquake input energy per unit mass (E_i/M) for various ductility demand ratios. For earthquake records developed for LA area the input energy spectra increase up to period of 1.5 second and decrease as period increases larger than 1.5 second. For period range less than approximately 0.5 second, input energy is not affected by ductility; however the input energy spectra decrease with the increase of ductility in period range longer than 0.5 second. Similar trend can also be observed in analysis results for earthquake records developed to be used in Boston area. It also can be observed that the variation of input energy depending on the change in ductility is larger in the region of high seismicity, LA area, and that in Boston area the input energy spectra are rapidly reduced in period longer than about 2 seconds. The input energy in soft soil condition is larger than that in other site conditions because the strong motion duration (t_{sd})

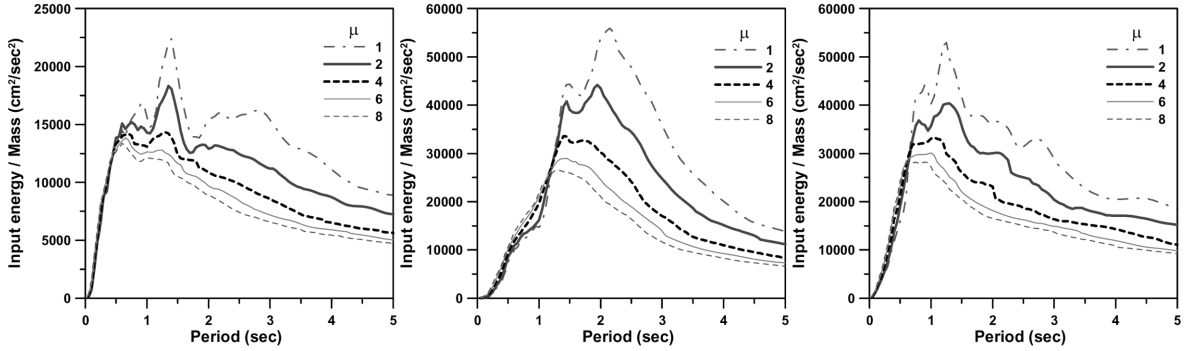

(a) Stiff soil (b) Soft soil (c) Near-fault

Fig. 4 Input energy spectra of ground motions for LA area

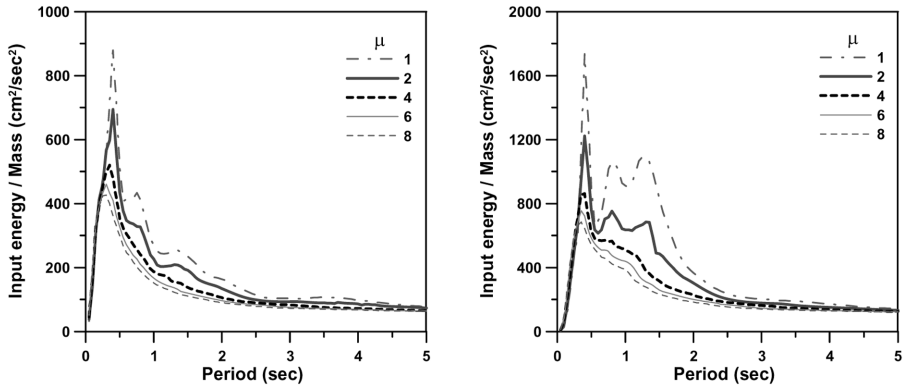

(a) Stiff soil (b) Soft soil

Fig. 5 Input energy spectra of ground motions for Boston area

for soft soil is larger than those of the other soil conditions.

Fig. 6 shows that the shapes of hysteretic energy vary depending on soil condition. For soils in LA area the spectrum is broad-banded in stiff soil, intermediate width-banded in soft soil and near-fault condition. However the hysteretic energy spectra of earthquakes for Boston area are narrow-banded. According to the figure, the hysteretic energy demand increases as the ductility ratio increases in short period region. On the other hand, this trend is reversed in the long period region of the energy spectra. As the target ductility ratio increases, the period at which this reversal occurs becomes shorter.

Excessive cumulative plastic deformations may lead to failure of structural members even when the deformations of members are considerably smaller than the ultimate deformation capacity of members under monotonic loading. This phenomenon cannot be estimated only by hysteretic energy (E_h). It can be evaluated by considering simultaneously the hysteretic energy, strength, and stiffness of the structure as follows (Teran-Gilmore and Jirsa 2004)

$$E_{hn} = \frac{E_h}{F_y \delta_y} \tag{7}$$

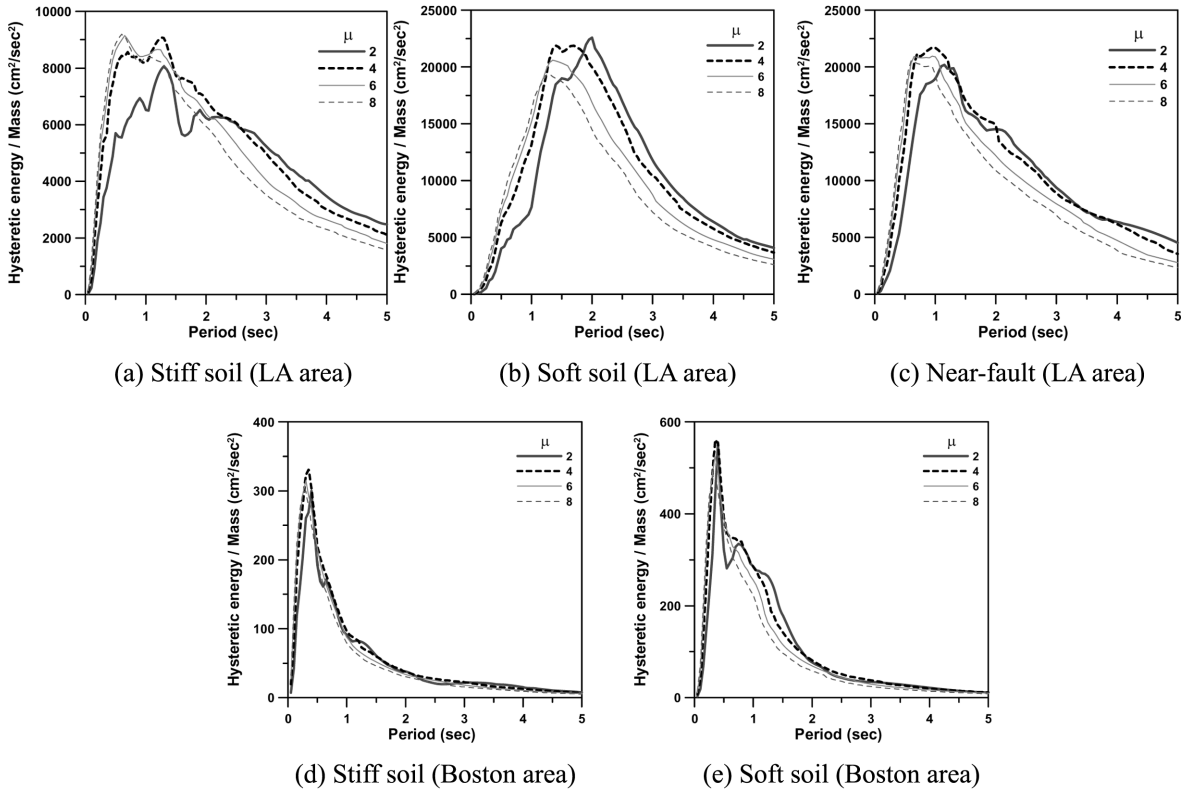

Fig. 6 Hysteretic energy spectra of ground motions for various ductility demands

where E_{hn} is normalized hysteretic energy. F_y and δ_y are the yield strength and yield displacement of the structure, respectively. For elastoplastic system subjected to ground motion, E_{hn} is the sum of plastic displacements normalized by δ_y in two opposite directions.

Normalized hysteretic energy demands for different soil conditions are depicted in Fig. 7. It can be observed that E_{hn} for each soil condition, except for soft soil in LA area, increases until the natural period (T) reaches around the dominant period of acceleration response spectrum as shown in Figs. 1 and 2. In structures with the natural period longer than 2 second, E_{hn} seems to be invariable. Teran-Gilmore and Jirsa (2004) found these trends of SAC records developed for stiff soil with 10% and 50% exceedance in 50 years. It also can be observed that E_{hn} for low seismicity (Boston area) is larger than those for high seismicity (LA area) although the contrary is observed in hysteretic energy spectra. The difference between normalized hysteretic energies for two areas increases as ductility demand increases.

In order to investigate the effect of the post-yield stiffness ratio on input and hysteretic energy, the energies of structures with post-yield stiffness of 0, 0.05, and 0.1 were estimated for the constant ductility demand of $\mu = 4.0$. Analysis results shown in Fig. 8 indicate that the post-yield stiffness ratio has negligible influence on the input and hysteretic energy. This result is similar to the observation reported by Zahrah and Hall (1984). They have concluded that post-yield stiffness ratio do not affect the input and hysteretic energy. Also Decanini and Mollaioli (2001) showed that for a structure on rock or stiff soil (S1) and intermediate soil (S2) the hysteretic behavior model does not lead to important variations in input energy response, on the other hand placing of a structure on

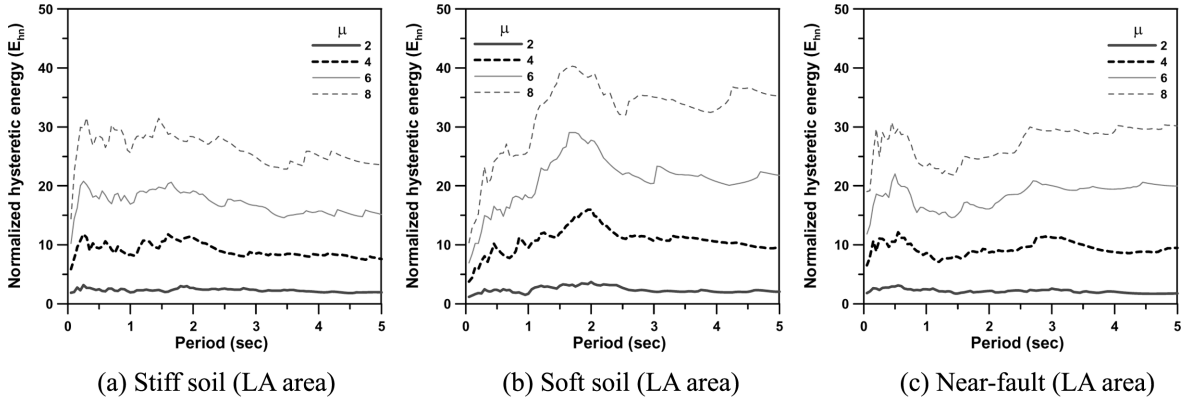

(a) Stiff soil (LA area) (b) Soft soil (LA area) (c) Near-fault (LA area)

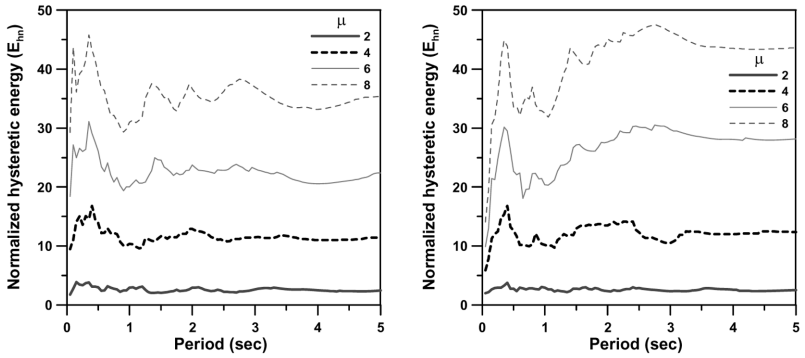

(d) Stiff soil (Boston area) (e) Soft soil (Boston area)

Fig. 7 Normalized hysteretic energy spectra of ground motions for various ductility demands

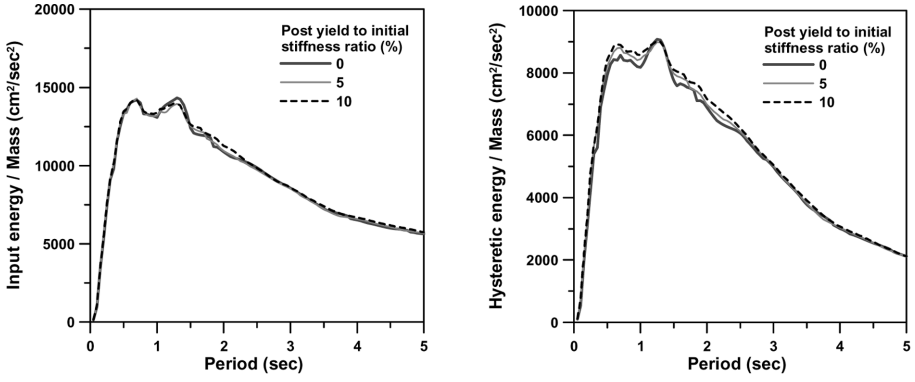

(a) Input energy (b) Hysteretic energy

Fig. 8 Change in input and hysteretic energy for various post-yield stiffness ratios (Stiff soil in LA area, $\mu = 4.0$)

soft soil (S3) makes the energy response highly sensitive to the hysteretic behavior type. But Nakashima *et al.* (1996) observed that the total input energy and hysteretic energy become less insensitive to the yield strength when the post-yield stiffness ratio increases as much as 0.75.

3.3 Ratio of hysteretic to input energy

Fig. 9 to Fig. 10 show that the ratio of the hysteretic to input energy (E_h/E_i) generally increases as the ductility ratio increases, but decreases as the natural period of the structure increases. As part of the input energy is also dissipated by damping, the hysteretic energy hardly exceeds about 70% of the input energy. It can be observed that, in high seismic region, the ratio remains near the upper bound for natural period less than about 2.5 second (Fig. 9(a)); however in low seismic region, the ratio decreases rapidly for natural period longer than about 1.0 second (Fig. 9(b)). It also can be noticed that in the long-period region of the spectrum the effect of ductility is insignificant because the ductility demand is small. Teran-Gilmore (1996) investigated the effect of strong motion duration on energy responses, and found that the size of plateau in E_h/E_i spectra tends to increase with an increase in strong motion duration and a decrease in ductility demand. Therefore it would be unreasonable or uneconomical to design a medium to high-rise structure to dissipate earthquake energy by plastic deformation. According to Fig. 10, the ratios in all site conditions are similar to one another regardless of the ductility demands for structures with natural period less than about 3

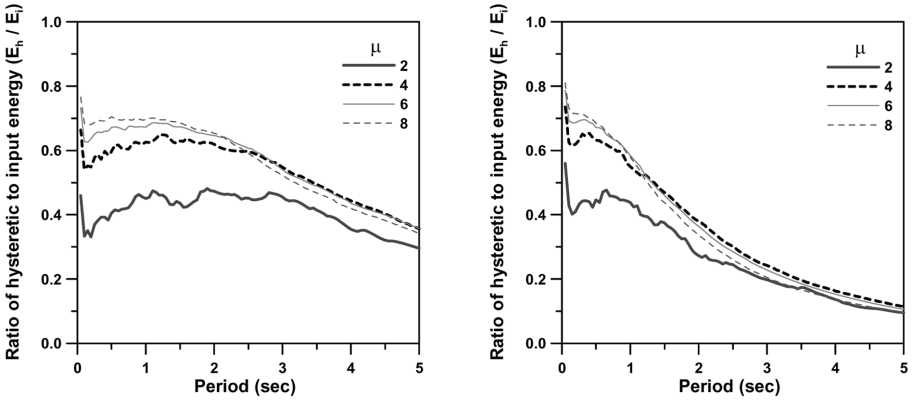

(a) Stiff soil (LA area) (b) Soft soil (Boston area)

Fig. 9 Ratio of hysteretic to input energy for various ductility demands

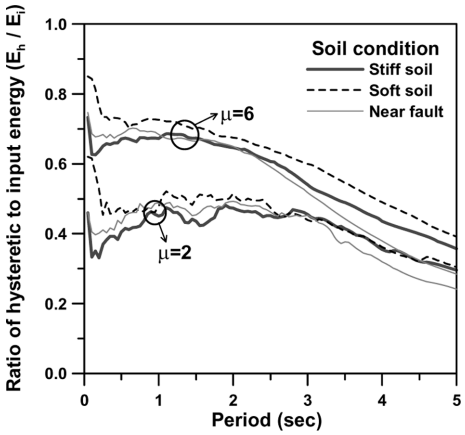

Fig. 10 Ratio of hysteretic to input energy for various soil conditions (LA area)

seconds, whereas the ratios of the records developed for near-fault condition become smaller than those of the records corresponding to the other site conditions when the natural periods are larger than 3 seconds. This result, however, does not correspond with the results of Khashaee *et al.* (2003) obtained using 20 records, which show that the ratios remain nearly constant when the ductility demand varies from 2 to 5. The discrepancy seems to be resulted from the fact that the energy ratios presented in their study were average values of the results computed using earthquakes with various soil conditions. Decanini and Mollaioli (2001) also found that the ductility ratio and the soil condition affect the ratio significantly.

Fig. 11 shows the ratios for earthquake records with long and short strong motion durations, which were presented in Table 1 and 2. It can be observed that the energy ratios remain stable for the records with long strong motion duration time, whereas the energy ratios decrease significantly in long period region when the earthquake records with relatively short strong motion duration are used in the analysis. Significant decrease of energy ratio in long period region with short strong motion duration results in rapid decrease of energy ratio as shown in Fig. 9. This implies that earthquakes with long strong motion duration inflict plastic deformation (damage) on structures with

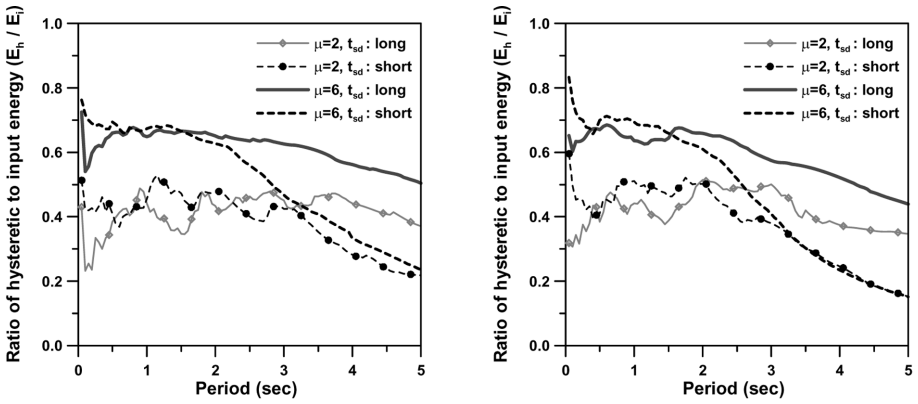

(a) Stiff soil (b) Near-fault

Fig. 11 Ratio of hysteretic to input energy for various ductility ratios and strong motion durations (LA area)

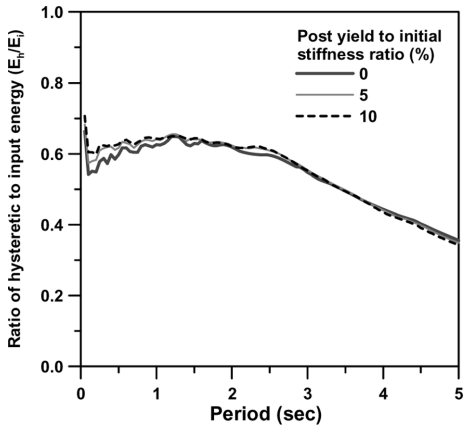

Fig. 12 Change in energy ratios (E_h/E_i) for various post-yield stiffness ratios (Stiff soil in LA area, $\mu = 4.0$)

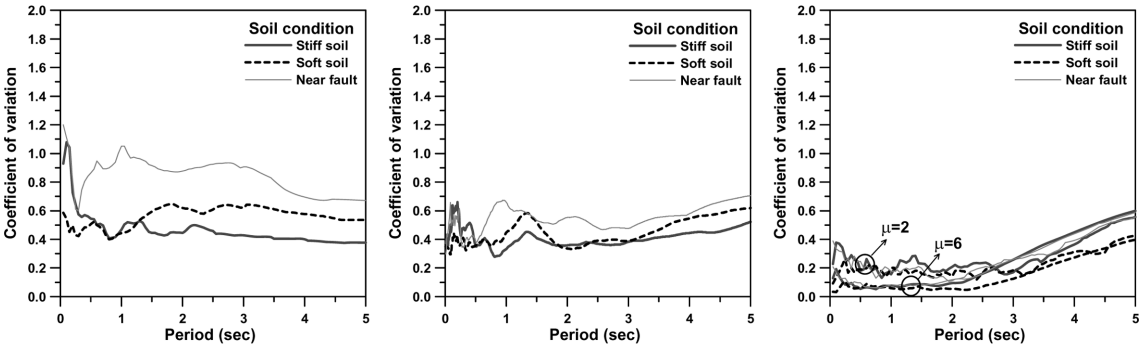

(a) Input energy for μ=6.0 (b) Acceleration response (c) Energy ratio (E_h / E_i)

Fig. 13 Coefficient of variation of energy and acceleration response (LA area)

wide spectrum of natural periods, whereas those with short strong motion duration damage structures with only short natural periods. Fig. 12 shows the effect of post-yield stiffness on the ratio, where it can be noticed that the ratio is not affected by the post-yield stiffness. Therefore it can be concluded that as the ratio remains stable regardless of the site conditions in structures with up to medium natural periods, the quantity can be used as a reliable design parameter in energy-based seismic design.

The coefficients of variation (COV) of responses, the standard deviations divided by the mean values, for the 20 earthquake records in each site condition are presented in Fig. 13. The COV of input energy shown in Fig. 13(a) are relatively constant for whole period range except for the periods less than 0.3 second. It can be observed that the COV for the near-fault and stiff soil records form upper and lower bounds, respectively. The larger COV for the near-fault records is contributed from the fact that the accelerograms recorded in near-fault usually have higher impulsive components. Similar trend can be observed in COV of acceleration response spectrum for 5% damping ratio as shown in Fig. 13(b), although the overall magnitudes of COV are generally smaller than those of input energy. The COV of the hysteretic to input energy ratio (E_h/E_i), shown in Fig. 13(c), turn out to be less sensitive to the site conditions and are smallest in magnitude. For natural period less than 2.5 second, the COV decrease as the ductility ratio increases. Although they increases as the natural period increases more than about 2.5 second, the analysis results imply that the hysteretic to input energy ratio can be considered as the most stable design parameter in the design of medium to low-rise structures.

4. Strength-based and energy-based seismic design

In section 3 it was shown that the normalized hysteretic energy did not vary significantly in most period ranges except short periods regardless of site conditions. It was also shown that the coefficient of variation of the hysteretic energy for input energy is small. These findings back up the validity of the energy-based design using hysteretic energy. In this section, structures with buckling restrained braces were designed and the seismic performances of the structures were compared with those of strength- designed structures.

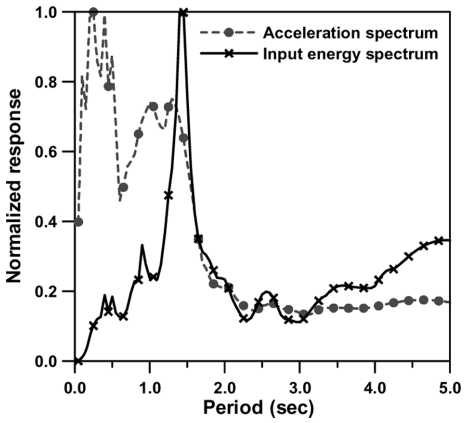

Fig. 14 Normalized pseudo-acceleration and input energy spectra of LA10 earthquake record

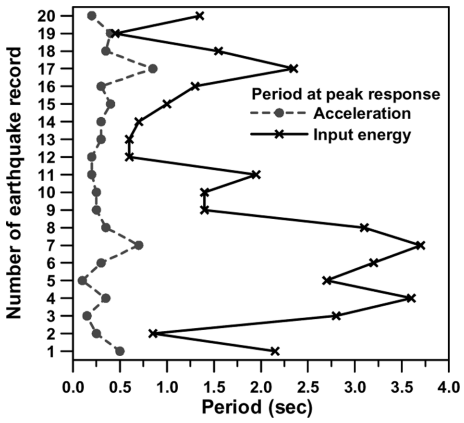

Fig. 15 Natural periods at maximum pseudo-acceleration and input energy spectra of stiff soil in LA area

Table 4 The dominant period of pseudo-acceleration and energy spectra

Area	LA			Boston	
Soil type	Stiff soil	Soft soil	Near-fault	Stiff soil	Soft soil
Pseudo-acceleration (sec)	0.31	0.50	0.73	0.15	0.37
Input energy (sec)	1.30	1.40	1.05	0.35	0.40
Hysteretic energy (sec)	1.25	1.40	0.95	0.35	0.35

4.1 Pseudo-acceleration and energy spectra

According to the pseudo-acceleration spectra of the ground motions used in the analyses (Fig. 1 and Fig. 2), the maximum values generally occur at the short-period region, except for a few earthquakes recorded at soft soil and near-fault region. Fig. 14 shows that in the pseudo-acceleration spectrum for the LA10 earthquake the maximum value corresponds to the natural period of 0.25 second, but that the maximum input energy occurs at the period of 1.4 second at which the relative velocity was maximized. Similar results were observed by Khashaee *et al.* (2003). Fig. 15 plots the natural periods at which the maximum pseudo-acceleration and input energy spectra occurred. It can be observed that the maximum pseudo-accelerations for the 20 earthquake records (LA area, stiff soil) occurred at quite similar natural periods. However in the case of input energy the maximum values occurred at longer natural periods. The dominant period of hysteretic energy spectrum is close to that of input energy spectrum. The natural periods corresponding to the maximum spectral values are summarized in Table 4, in which it can be observed that the natural periods at the maximum energy responses are about two to four times longer than those at the maximum pseudo-acceleration, except for soft soil in Boston area. This implies that the structural design based on the input or hysteretic energy may not satisfy the strength demands.

4.2 Design of model structures

According to previous research (Black *et al.* 2002, Merritt *et al.* 2003), a BRB exhibits a stable

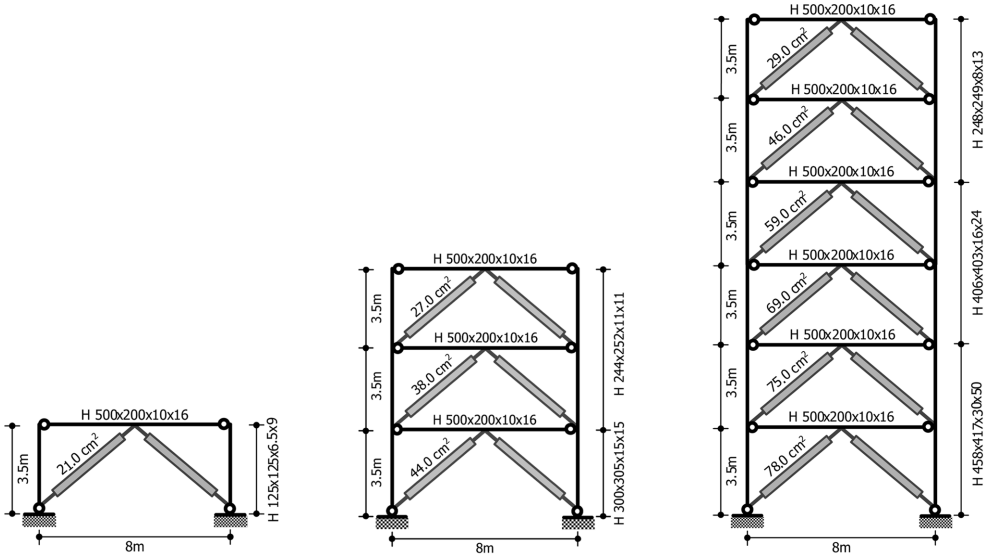

(a) One-story structure (b) Three-story structure (c) Six-story structure

Fig. 16 Model structures designed based on strength

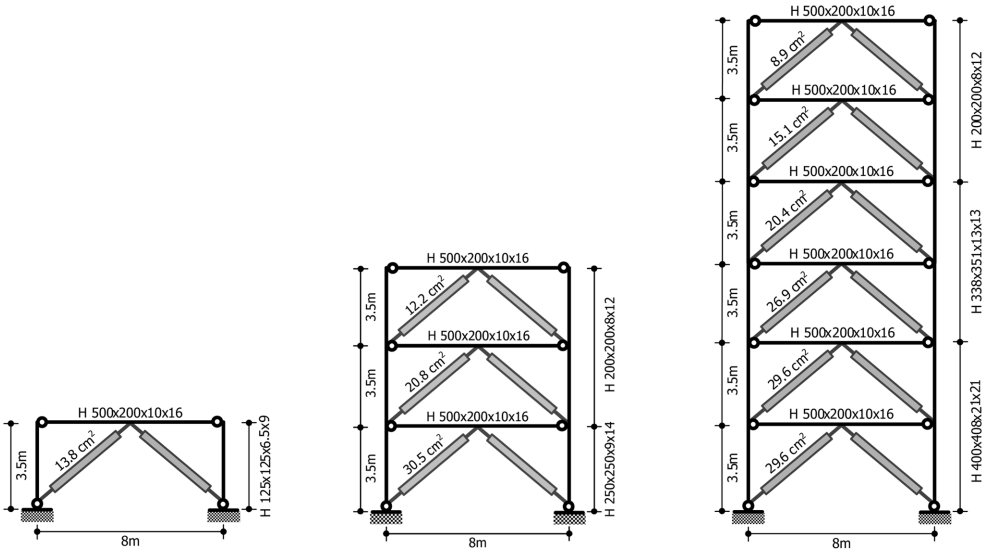

(a) One-story structure (b) Three-story structure (c) Six-story structure

Fig. 17 Model structures designed based on energy

hysteretic behavior with excellent energy dissipation capacity both in tension and compression. A steel casing and mortar filler are used to provide lateral support to the core element and to prevent global and local buckling of the steel core when compressive force is applied. Consequently the hysteretic behavior of BRB can easily be modeled and the amount of dissipated energy can be computed using simple equations (Choi *et al*. 2006b). To compare the seismic performance of structures designed based on both strength and energy, buckling-restrained braced frames (BRB)

were prepared. The 1, 3, and 6 story-structures have 3.5m story height and 8m bay length. As shown in Figs. 16 and 17 the girders are pin-connected to columns, and only the BRBs dissipate seismic energy through plastic deformation. The design dead and live loads of 4.9kN/m^2 and 2.45kN/m^2, respectively, were used for design. The inherent modal damping ratios for dynamic analysis were assumed to be 5% of the critical damping in the first and the second modes.

For strength based design of BRB frames, the seismic load was computed using the mean response spectrum presented in Fig. 1(a), in which the seismic coefficients S_{DS} and S_{D1} in the IBC 2006 format are estimated to be 1.375 and 0.77, respectively. The importance factor of 1.25 was used to obtain design base shear. Beams and columns were designed per the AISC Load and Resistance Factor Design (1999) and the Seismic Provisions for Structural Steel Buildings (2002). The BRBs were designed per Chapter 8 of the FEMA-450 (BSSC 2004), in which the response modification factor of buckling-restrained braced frames is specified as 7. The yield stress of the structural steel is 240 MPa. In the strength-based design the ratio of stress demand to capacity is kept above 0.9 for beams and columns and especially above 0.95 for BRBs. The steel core areas of BRBs were calculated using the following relation suggested in the FEMA-450

$$P_u \le \phi P_{ysc} \tag{8}$$

where P_u is the required axial strength and ϕ is the strength reduction factor, which is 0.9. $P_{ysc} = F_y A_{sc}$ is the design strength, where F_y and A_{sc} are the specified minimum yield strength and net area of steel core, respectively.

For energy based design of BRB frame, the procedure proposed previously by the authors (2006a) was followed: The target displacement (1.5% of story height) and the ductility ratio ($\mu_t = 6.5$ for all stories) at the target displacement were determined first. Then the hysteretic energy spectrum and the accumulated ductility spectrum corresponding to the ductility ratio (μ_t) were constructed, and the hysteretic energy (E_h) and the accumulated ductility ratio (μ_a) corresponding to the natural period of the model structures were obtained. The accumulated ductility ratio μ_a is the sum of the positive and negative yield excursions. By assuming that all the seismic input energy is dissipated by BRBs, the cross-sectional area of BRBs located in the first story can be computed as follows

$$E_h \times \sum_{i=1}^{N} m_i = \sum_{j=1}^{N} F_{yj} u_{yj} (\mu_a - 1) = (\mu_a - 1) \sum_{j=1}^{N} A_{bj} \sigma_{by} \frac{L_{bj} \sigma_{by}}{E_b} \tag{9a}$$

$$A_{b1} = \frac{E_h \sum_{i=1}^{N} m_i}{(\mu_a - 1) \sum_{j=1}^{N} D_j \sigma_{by} \frac{L_{bj} \sigma_{by}}{E_b}} \tag{9b}$$

where E_h, F_{yj}, u_{yj}, and μ_a are the hysteretic energy normalized by mass obtained from the spectrum, the yield force of the jth story, the yield displacement of the jth story, and the accumulated ductility ratio, respectively. For model structures the values of μ_a range approximately from 20 to 23. Also A_{bj} and L_{bj} are the cross-sectional area and length of BRB located on the jth story, respectively. σ_{bj} and E_b are yield stress and elastic modulus of BRB, respectively. m_i is the mass of the ith story. The cross-sectional area of BRB located in the jth story, A_{bj}, is denoted as the cross-sectional area of BRB in the first story, A_{b1}, multiplied by the story-wise distribution ratio, D_j

$$A_{bj} = D_j A_{b1} \tag{10}$$

In this study it is assumed that the hysteretic energy is distributed in each story proportional to the story-wise distribution ratio of hysteretic energy obtained from nonlinear dynamic analysis. Figs. 16 and 17 show the size of structural members selected using the code-based and the energy-based procedures, respectively.

4.3 Seismic performance of model structures

Fig. 18 shows the pseudo accelerations and the hysteretic energy demands ($\mu_t = 6.5$) of model structures averaged over the results for the 20-earthquake records used previously. The parenthesized values in the figure are natural periods of model structures using energy based design (EBD) and strength based design (SBD), respectively. For the given model structures, the acceleration demand, which was used for strength-based design of model structures, decreases as the number of story increases, whereas the energy demand increases as the number of story increases.

Fig. 19 presents the pushover curves of the model structures. The nonlinear analysis code DRAIN-2D+ (Tsai and Li 1997) was used in the analysis. The post-yield stiffness of beams and columns are assumed to be 2% of the initial stiffness, and that of the BRB is assumed to be zero. It is also assumed that yield stress of BRB is equal in both tension and compression. In the curves it can be observed that the yield strength of structures designed based on energy is much smaller than that of the structures designed based on strength. The base shears at yield of the one and the six

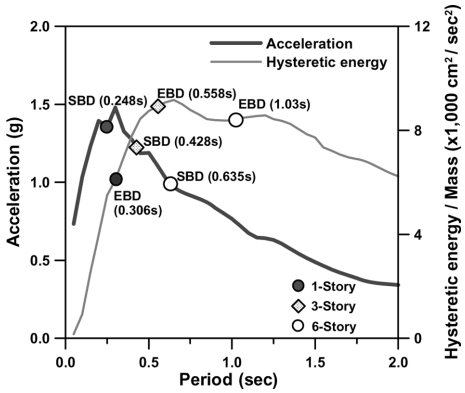

Fig. 18 Pseudo-accelerations and hysteretic energy demands of model structures

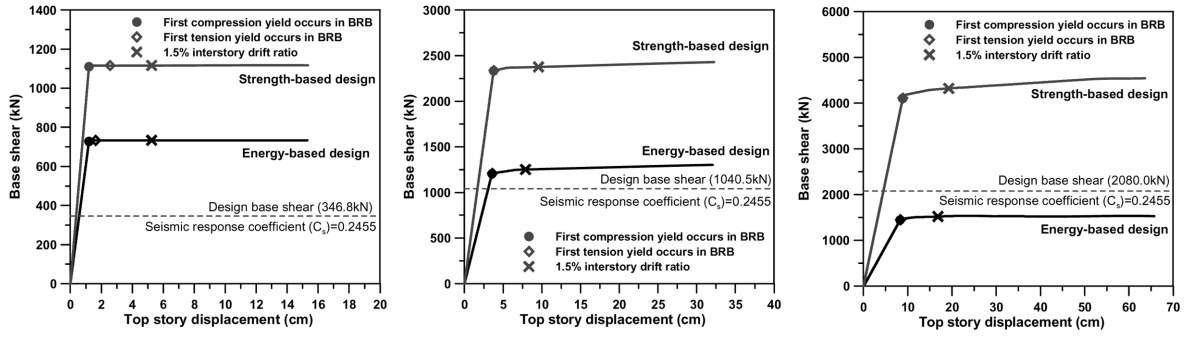

(a) One-story structure (b) Three-story structure (c) Six-story structure

Fig. 19 Pushover curves of the model structures

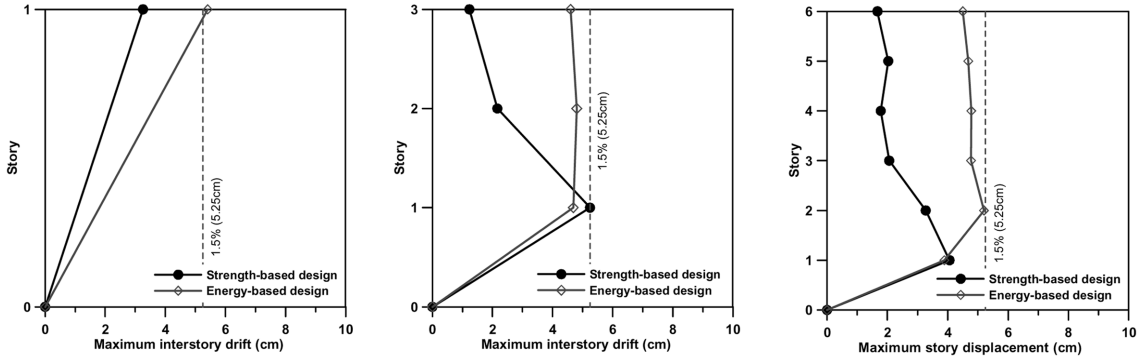

(a) One-story structure (b) Three-story structure (c) Six-story structure

Fig. 20 Maximum inter-story drifts of the model structures

story energy-designed structures are only 66% and 35%, respectively, of the strength-designed structures. The over-strength factors, the ratio of the yield to design stress, are 3.20 (1-story), 2.24 (3-story), and 1.97 (6-story) for strength-designed structures, which are larger than or equal to the over-strength factor of 2.0 specified in the FEMA-450 (BSSC 2004). However the over-strength factors of the structures designed based on energy are 2.10 (1-story), 1.16 (3-story), and 0.69 (6-story), which are significantly smaller than those of the strength-designed structures. The smaller overstrength factors of the structures designed based on energy are partly contributed from the fact that the structures are more optimally designed in such a way that structural damages are more uniformly distributed throughout the stories. Another important factor is that the strength reduction factors and load factors were not used in the energy-based design, whereas they were applied in the code-based strength-design.

Fig. 20 shows the maximum inter-story drifts of the model structures obtained from time-history analysis. The mean values for the 20 earthquake records (stiff soil in LA area) were plotted in the figure. The dotted vertical lines represent the target displacements (1.5% of story height). It can be observed that the energy-designed structures generally meet the target displacements as the structures were designed so that the input energy and the hysteretic energy are balanced at the target displacement. The inter-story drifts of structures designed based on strength, however, are much less than the target displacements. The inter-story drifts are largest in the first story, which implies that large damage is concentrated there, whereas in energy-based design lesser damage is distributed throughout the stories. It should be pointed out that the structures may suddenly collapse due to lack of redundancy if the story-wise inelastic damage is nearly uniform. This, however, may be a trade-off of an optimum design. In practice, moment-resisting frames are frequently added to the buckling-restrained braced frames to ensure safety against large earthquakes.

The energy responses of the model structures are presented in Table 5. There is small difference between the input energies for strength- and energy-designed structures except for the 1-story structures. However the ratios of the hysteretic to input energy (E_h/E_i) of the energy-designed structures are generally larger than those of the strength-designed structures. Large story ductility results in large energy ratio E_h/E_i. In the 6-story structure the story ductility ratios for strength- and energy-designed structures were 2.07~5.07 and 4.82~6.4, respectively. The rest of the input energy ($1 - E_h/E_i$) is dissipated by damping. It can be found that the energy ratios (E_h/E_i) for buildings with different heights are similar as depicted in Fig. 9(a).

Table 5 Energy responses of model structures

Story	Strength based design		Energy based design	
	Input energy/mass (cm^2/sec^2)	E_h/E_i	Input energy/mass (cm^2/sec^2)	E_h/E_i
1 Story	7024	0.446	9251	0.596
3 Story	10615	0.504	11345	0.647
6 Story	12099	0.460	11624	0.654

5. Conclusions

In this study the influences of ground motion characteristics and structural properties on energy demands were evaluated using 100 earthquake ground motions recorded in different soil conditions, and the results were compared with those of previous works. Then framed structures with buckling-restrained-braces (BRBs) were designed in such a way that all the input energy is dissipated by the hysteretic energy of the BRBs, and the results were compared with those designed by conventional strength-based design procedure.

The analytical results showed that ductility ratios and the site conditions had significant influence on the input energy. The ratio of hysteretic to input energy was considerably affected by the ductility ratio and the strong motion duration. The evaluation of normalized hysteretic energy demands (E_{hn}) for different soil conditions showed that E_{hn} for low seismicity (Boston area) was larger than those for high seismicity (LA area) although the opposite was observed in hysteretic energy spectra. Therefore hysteretic energy in itself may not provide enough information about the damage caused by accumulated yield excursions. In the comparison of pseudo-acceleration and energy spectra, it was found that the natural periods corresponding to the maximum energy response were about two to four times longer than those at the maximum pseudo-acceleration. This implies that the structural design based on the energy demand may not satisfy the strength demand. The static and dynamic nonlinear analyses of both strength-designed and energy-designed structures showed that the energy-based design, which is basically performance-based, resulted in smaller member size, smaller strength, and more damage compared to structures designed based on strength. Therefore if a structure, designed based on energy, is to meet both strength and displacement criteria, it is necessary to check strength after it is designed based on energy, as the strength-based design requires displacement check afterwards.

References

AISC (1999), *Load and Resistance Factor Design Specification for Structural Steel Buildings*, American Institute of Steel Construction, Chicago, IL.

AISC (2002), *Seismic Provisions for Structural Steel Buildings*, American Institute of Steel Construction, Chicago, IL.

Akbas, B. (2006), "A neural network model to assess the hysteretic energy demand in steel moment resisting frames", *Struct. Eng. Mech.*, **23**(2), 177-193.

Akbas, B., Shen, J. and Hao, H. (2001), "Energy approach in performance-based seismic design of steel moment resisting frames for basic safety objective", *Struct. Des. Tall Build.*, **10**(3), 193-217.

Akiyama, H. (1985), *Earthquake-resistant Limit-state Design for Buildings*, University of Tokyo Press, Japan.

Arias, A. (1970), "A measure of earthquake intensity", in Seismic Design for Nuclear Power Plants, ed. R.J.

Hansen, Massachusetts Institute of Technology Press, 438-469.
Black, C., Makris, N. and Aiken, I. (2002), "Component testing, stability analysis and characterization of buckling restrained braces", PEER Report 2002/08, Pacific Earthquake Engineering Research Center, University of California, Berkeley.
Bojórquez, E. and Ruiz, S.E. (2004), "Strength reduction factors for the Valley of Mexico, considering low-cycle fatigue effects", *13th World Conference on Earthquake Engineering*, Vancouver, Canada, Paper No. 516.
Bruneau, M. and Wang, N. (1996), "Some aspects of energy methods for the inelastic seismic response of ductile SDOF structures", *Eng. Struct.*, **18**(1), 1-12.
Building Seismic Safety Council (2004), "NEHRP Recommended provisions for seismic regulations for new buildings and other structures, 2003 Edition, Part 1: Provisions", Report No. FEMA-450, Federal Emergency Management Agency, Washington, D.C.
Choi, H. and Kim, J. (2006a), "Energy-based seismic design of buckling-restrained braced frames using hysteretic energy spectrum", *Eng. Struct.*, **28**(2), 304-311.
Choi, H., Kim, J. and Chung, L. (2006b), "Seismic design of buckling-restrained braced frames based on a modified energy-balance concept", *Can. J. Civil Eng.*, **33**(10), 1251-1260.
Chopra, A.K. (1995), *Dynamics of Structures: Theory and Applications to Earthquake Engineering*, Prentice Hall Inc., New Jersey.
Cruz, M.F. and López, O.A. (2000), "Plastic energy dissipated during an earthquake as a function of structural properties and ground motion characteristics", *Eng. Struct.*, **22**(7), 784-792.
Decanini, L.D. and Mollaioli, F. (2001), "An energy-based methodology for the assessment of seismic demand", *Soil Dyn. Earthq. Eng.*, **21**(2), 113-137.
Fajfar, P. and Vidic, T. (1994), "Consistent inelastic design spectra: Hysteretic and input energy", *Earthq. Eng. Struct. Dyn.*, **23**(5), 523-537.
Housner, G.W. (1956), "Limit design of structures to resist earthquakes", *Proceedings of the First World Conference on Earthquake Engineering*, Berkeley, California.
ICC (2006), *2006 International Building Code*, International Code Council Inc., Country Club Hills, IL.
Khashaee, P., Mohraz, B., Sadek, F., Lew, H.S. and Gross, J.L. (2003), "Distribution of earthquake input energy in structures", Report No. NISTIR 6903, National Institute of Standards and Technology, Washington.
Kim, J., Choi, H. and Chung, L. (2004), "Energy-based seismic design of structures with buckling-restrained braces", *Steel Compos. Struct.*, **4**(6), 437-452.
Leelataviwat, S., Goel, S.C. and Stojadinovi, B. (2002), "Energy-based seismic design of structures using yield mechanism and target drift", *J. Struct. Eng.*, **128**(8), 1046-1054.
Mahin, S.A. and Lin, J. (1983), "Inelastic response spectra for single degree of freedom systems", Department of Civil Engineering, University of California, Berkeley.
Merritt, S., Uang, C.M. and Benzoni, G. (2003), "Subassemblage testing of corebrace buckling-restrained braces", Report No. TR-2003/01, University of California, San Diego.
Nakashima, M., Saburi, K. and Tsuji, B. (1996), "Energy input and dissipation behaviour of structures with hysteretic dampers", *Earthq. Eng. Struct. Dyn.*, **25**(5), 483-496.
Somerville, P., Smith, H., Puriyamurthala, S. and Sun, J. (1997), "Development of Ground Motion Time Histories for Phase 2 of the FEMA/SAC Steel Project", SAC Joint Venture, SAC/BD 97/04.
Teran-Gilmore, A. (1996), "Performance-based earthquake-resistant design of framed buildings using energy concept", *Ph. D. Thesis*, University of California at Berkeley.
Teran-Gilmore, A. and Jirsa, J.O. (2004), "The use of cumulative ductility strength spectra for seismic design against low cycle fatigue", *13th World Conference on Earthquake Engineering*, Vancouver, Canada, Paper No. 889.
Trifunac, M.D. and Brady, A.G. (1975), "A study on the duration of strong earthquake ground motion," *B. Seismol. Soc. Am.*, **65**(3), 581-626.
Tsai, K.C. and Li, J.W. (1997), "DRAIN2D+, A general purpose computer program for static and dynamic analyses of inelastic 2D structures supplemented with a graphic processor", Report No. CEER/R86-07, National Taiwan University, Taipei, Taiwan.
Uang, C.M. and Bertero, V.V. (1988), "Use of energy as a design criterion in earthquake-resistant design", Report No. UCB/EERC-88/18, Earthquake Engineering Research Center, University of California at Berkeley.
Zahrah, T. and Hall, J. (1984), "Earthquake energy absorption in SDOF structures", *J. Struct. Eng.*, **110**(8), 1757-1772.